Wiley Online Library
Early View publication on www.wileyonlinelibrary.com
(issue and page numbers not yet assigned;
citable using Digital Object Identifier – **DOI**)

Laser Photonics Rev., 1600187 (2017) / **DOI** 10.1002/lpor.201600187

LASER & PHOTONICS REVIEWS

Abstract Multi scale hierarchical structures underpin mechanical, optical, and wettability behavior in nature. Here we present a novel approach which can be used to mimic the natural hierarchical patterns in a quick and easy mask-less fabrication. By using two-beam interference lithography with angle-multiplexed exposures and scanning, we have successfully printed large-area complex structures having a cascading resolution and 3D surface profiles. By precisely controlling the exposure dose we have demonstrated a capability to create different 3D textured surfaces having comparable aspect ratio with period spanning from 4 μm to 300 nm (more than one order of magnitude) and the height spanning from 0.9 μm to 40 nm, respectively. Up to three levels of biomimetic hierarchical structures were obtained that show several natural phenomena: superhydrophobicity, iridescence, directionality of reflectivity, and polarization at different colors.

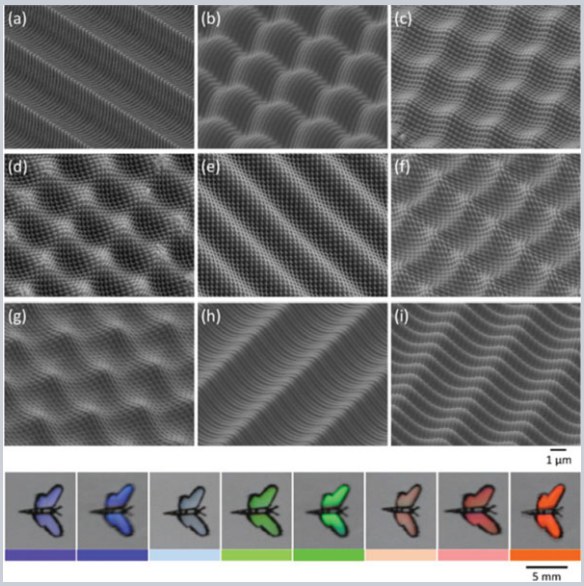

ORIGINAL PAPER

Angle-multiplexed optical printing of biomimetic hierarchical 3D textures

Muhammad Irfan Abid[1], Lei Wang[1], Qi-Dai Chen[1,*], Xue-Wen Wang[3,4], Saulius Juodkazis[1,3,4,*], and Hong-Bo Sun[1,2,*]

1. Introduction

Multi scale hierarchical structures underpin mechanical, optical, and wettability behavior in nature [1–12]. Most of the fabrication procedures developed so far to mimic natural hierarchy have experimental complexity and limited flexibility in structure symmetry [13–20], limitations in upscaling over extended macroscopic areas and lack of capability to structure 3D surfaces. Here, we show that using the angle-multiplexed exposure of two beam laser interference (2BI), hence a period modulation, combined with a lateral scan and precise exposure dose control, an endless variety of hierarchical 3D surfaces with features spanning over an order of magnitude in period and height made on micro-scaled surfaces with different geometrical symmetries can be laser printed. Using this technique we have successfully demonstrated hierarchical surfaces which mimic the wetting properties [21, 22] of natural plant leaves, optical properties of iridescence [23, 24], directionality of reflection and polarization of colors [15, 25] exhibited in nature. The most significant advantage of our technique over the other surface patterning methods is that it is mask-less and offers the flexibility to change the geometrical arrangement and axial symmetry of both micro and nanoscale surface patterns effortlessly. Another salient feature of our method is that within a time of few seconds $\sim 5 \times 5$ mm^2 region can be enlarged into areas with centimeter cross sections by sample translation which enables the mass production.

Many functions and properties exhibited by objects in nature are result of hierarchical ordering of micro/nanoscale structures and patterns by arranging simpler structures. The self-cleaning surface of lotus leaf [1], the reduced drag and hydrodynamics surface of a shark skin [2,3], the anisotropic wetting surface of a rice leaf [4, 26], the highly adhesive, superhydrophobic and surface enhanced Raman scattering substrate of a rose petal [5, 6], the water repellent legs of a water strider [7, 8], the anti-fogging compound eyes of mosquito [9] and fly [27], a reversible adhesion of a gecko's foot [10, 28], and structural colors of moths, butterflies [11] and bird feathers [12] are examples that have been

[1] State Key Laboratory on Integrated Optoelectronics, College of Electronic Science and Engineering, Jilin University, 2699 Qianjin Street, Changchun, 130012, China
[2] College of Physics, Jilin University, 2699 Qianjin Street, Changchun, 130023, China
[3] Centre for Micro-Photonics, Faculty of Science, Engineering and Technology, Swinburne University of Technology, Hawthorn, VIC, 3122, Australia
[4] Melbourne Centre for Nanofabrication, ANFF, 151 Wellington Road, Clayton VIC, 3168, Australia
M. I. Abid and L. Wang contributed equally to this work.
*Corresponding author(s): e-mail: hbsun@jlu.edu.cn, chenqd@jlu.edu.cn and saulius.juodkazis@gmail.com

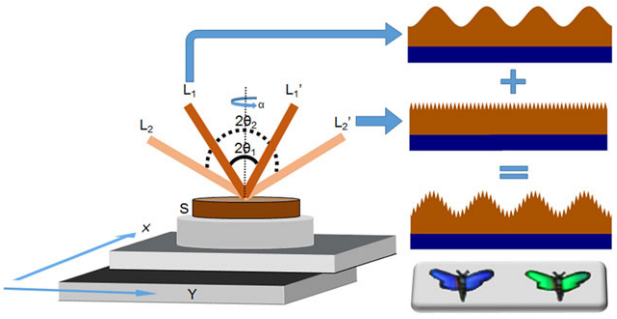

Figure 1 Schematic of angle varied multiple exposure of 2BI process. The schematic showing dependence of the grating period on the angle of two interfering beams. The beams L1-L1' with smaller angle $2\theta_1$ form a larger period (primary pattern), whereas the beams L2-L2' with a larger angle $2\theta_2$ form the smaller period (secondary pattern) on the substrate (S). The sequential combination of two periods produces the hierarchical structure. The substrate is mounted on a turn table which can be rotated at an angle (α) to achieve different patterns. Colors of butterfly wings were obtained as shown in the bottom right.

the source of motivation to follow the nature's rule of hierarchy for useful functions [24, 29–31].

Usually to make a hierarchical pattern, a microstructured surface is fabricated in the first step and then further processing is carried out to add nano-features over it at the second step [13, 18–20] by combining different fabrication techniques with different resolutions [32–35] making a whole process long, complicated and limited to a certain geometrical shape.

In this paper, we present a novel approach which can be used to mimic the natural hierarchical patterns in a quick and easy maskless process. A simple expose-scan experimental setup is required to laser-print a complex structure with cascading resolution and 3D surface profile. It is based on simplified multi-beam interference lithography (MBI) [36] with only two beams (2BI) [37, 38]. We added angle-multiplexed exposures and scanning to achieve flexibility and larger area coverage as shown in Fig. 1 (see Supplement for details). By precise exposure dose control, we demonstrate a capability to create 3D textured surfaces with period spanning more than one order of magnitude (4 – to - 0.3 μm) while keeping the same aspect ratio of different patterns with height spanning 0.9 –to- 0.04 μm. This is achieved using long nanosecond laser pulses and benefiting from a literally unlimited depth of the interference pattern into the depth of the sample. This is the key to writing on existing 3D surface created by multiplexed exposures, the newly demonstrated capability of 2BI.

2. Experimental section

The glass substrates were first cleaned with acetone and absolute ethanol and then rinsed with de-ionized water. The BP-212 positive photoresist (Beijing Institute of Chemical Reagents) was spin coated at 3000 rpm on the substrates for a thickness of about 3 μm. The glass substrates were then prebaked on a hotplate at 110°C for 60 seconds. The substrates were cooled to the room temperature before exposure. The laser beam from a frequency-tripled, Q-switched, single-mode Nd:YAG laser (Spectra-physics) with about 10 ns pulse width and 355 nm wavelength was split into two beams. The two-beam laser interference setup was made as shown in Supplementary Figure S1. For the primary patterns of 3 μm period the power of ~9 mm diameter laser beam was set to 300 mW whereas for secondary patterns of 300 nm the power was reduced to 200 mW. The exposure time in all the cases was one second. The samples were then developed in a 0.2% (w/v) aqueous solution of NaOH for about 3 to 5 minutes. The morphologies of the structures were studied using Field-emission SEM (JSM-7500F, JEOL, Japan) and AFM (Digital Instruments Nanoscope IIIA) in the tapping mode. Contact Angle was measured using an OCA 20 system (Data physics GmbH, Germany) at room temperature with droplet of about 0.5 μl. The images of the iridescence from structures were taken using a digital camera. For measuring the optical reflectivity and polarization characteristics, a 633-nm semiconductor laser light source was used.

3. Results and discussion

Various combinations of one, two and three exposures for each period with different axial symmetries between the primary and secondary patterns from 3 μm to sub-wavelength 300 nm are shown in scanning electron microscopy (SEM) images in Fig. 2. Heights of the primary and secondary patterns depend on the exposure dose (Supplementary Figure S3 and Fig. 3) and are from 700 nm to 900 nm for the primary and 50 nm to 100 nm for the secondary exposures, respectively. The secondary pattern could be fabricated at an arbitrary angle relative to the primary one (Fig. 2(c–g)). These results demonstrate versatility and flexibility of printing in which any symmetry (1D grating, 2D square, 2D hexagonal) can be made either at the primary or secondary level with an added flexibility of a phase shift in the axial orientation.

Further demonstration of capabilities of the proposed printing method is presented next with three levels of hierarchical patterning (Fig. 2(h–i)). Three periods of 4 μm, 1 μm and 300 nm were combined in the first, second and third patterns. Exposure doses of second and third levels were optimized to be lower as compared to the first level of gratings. This results in a structure having a surface texture of a 3-level hierarchy (Supplementary Table S1 shows details). Due to a shallower depth of structures with a smaller period, it was important to keep the following exposure sequence: first, exposure of the lager period (deeper pattern) and, second, the smaller period patterns. The exposed resist had a weaker absorption and this facilitated fabrication of deep patterns with alternating periods using multiple exposures.

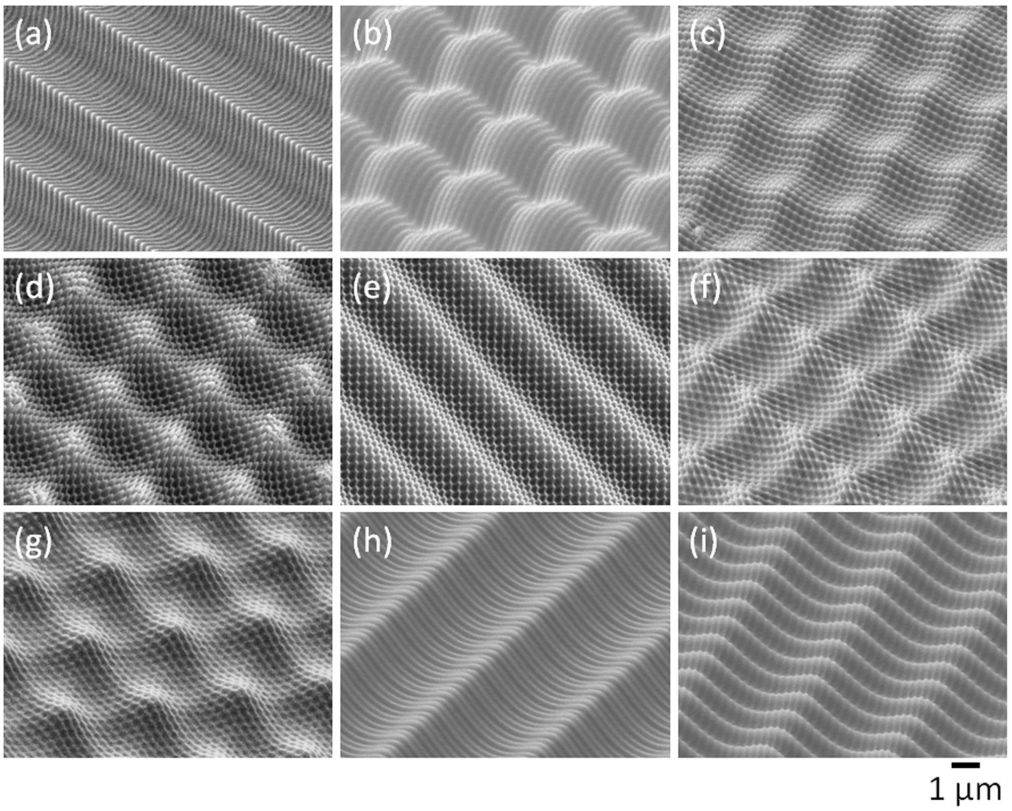

Figure 2 SEM micrographs of surfaces fabricated by multiple exposure of angle varied 2BI. From (a) to (i) the variations in the morphologies of the surface patterns show the capability of the process: (a) 300 nm 1D grating at 90° orientation w.r.t. 3 μm 1D grating; (b) 300 nm 1D grating at 0° orientation w.r.t. 3 μm 2D square patterns; (c) 300 nm 2D square pattern at 0° orientation w.r.t. 3 μm 2D square pattern; (d) 300 nm 2D square pattern at 45° orientation w.r.t. 3 μm 2D square pattern; (e) 300 nm 2D square pattern at 45° orientation w.r.t. 3 μm 1D grating; (f) 300 nm 2D hexagonal pattern at 0° orientation w.r.t. 3 μm 2D square pattern; (g) 300 nm 2D hexagonal pattern at 0° orientation w.r.t. 3 μm 2D hexagonal pattern; (h) 300 nm and 1 μm 1D gratings at 90° orientation w.r.t. 4 μm 1D gratings; (i) 1 μm 1D gratings at 90° orientation w.r.t. 300 nm and 4 μm 1D gratings. The scale bar in all images is 1 μm.

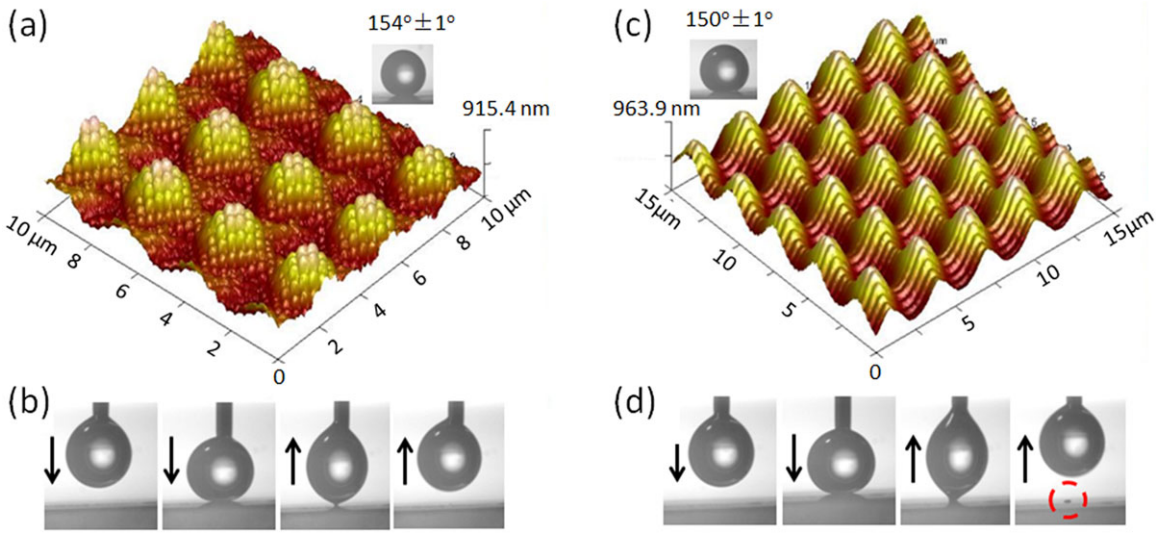

Figure 3 Wetting properties of hierarchical surfaces: (a) and (c) show the static contact angles of a droplet of water on the hierarchical surfaces shown in 3D AFM images; (b) and (d) show the series of images (from left to right) when 0.5 μl droplet of water approaches the surface, touches it and then is pulled back from the surface of the structures of (a) and (c), respectively. The red circle in (d) shows the little amount of water left on the surface in (c) due to stronger adhesion of the water droplet to the surface. The arrows indicate direction of motion of the droplet.

It is demonstrated next, that printed hierarchical micro-nano-structured surfaces can mimic the wettability of natural leaves [1,22,39] and achieve super hydrophobicity with a contact angle $\theta >> 150°$. Printed surfaces were treated with fluoroalkylsilane to add chemical hydrophobicity in addition to that caused by structure. The static water contact angle on the structure which resemble the surface morphology of the leaf of hygoryza aristata [21] (Fig. 2 (d)) is shown in Fig. 3(a). The flat substrate surface had the contact angle $\theta = 114°$, the surface with only primary square 2D pattern of pins with 3μm period exhibited 130°, and even a larger static $\theta = 138°$ was observed on the similar surface of 300 nm period (supplementary Figure S4). The contact angle increased to 154° (Fig. 3(a)) for the hierarchical structure shown in Fig. 2(d).

Different surface wettability is underpinned by the chemical and structural composition of the surface. If the liquid and solid contours exactly connect to each other and liquid completely fills the valleys between the peaks of a rough surface, this corresponds to the Wenzel case with the contact angle [40]:

$$\cos\theta = r\cos\theta_o, \quad (1)$$

where r is the roughness factor defined as the ratio of the actual surface area to the projected area, and θ_o is the contact angle on the flat surface of the same material. For the hierarchical texture shown in Fig. 2(d), the factor r = 1.45 was measured directly from the AFM map over area of 10 μm × 10 μm. With $\theta_0 = 114°$, it was found that $\theta = 126°$ is expected (Equation (1)). However, the experimentally measured contact angle was larger. The Cassie-Baxter (CB) model [41] was applied where the droplet only resides on the peaks over a rough surface, forming air pockets between liquid and solid with the contact angle governed by:

$$\cos\theta = f_s(\cos\theta_o + 1) - 1, \quad (2)$$

where f_s is the fractional contact area between the liquid and the solid. For the Fig. 2(d) texture with $\theta = 154°$ and θ_o= 114°, the value of solid fraction f_s was evaluated as 0.17.

When nanostructures form continuous grating lines on the top of 2D micro structures (Fig. 2(b)) the wetting behavior is different. The contact angle of this surface was $\theta = 150°$ (Fig. 3(c)), only slightly lower as compared to that of the structure in Fig. 2(d). The increased solid fraction f_s was observed in this case. The following test revealed dynamic behavior of wetting with droplet gradually sinking into the structure until it touched the bottom surface. It did not spread out even when it was firmly touched to the bottom surface. When dragged over the surface (Fig. 2(d)), the drop did not stick to the surface either and was easily detached when raised up with the needle. In the case of surface shown in Fig. 2(b), the droplet showed a stronger adhesion (Fig. 3) while a small amount of water was left on the surface after detachment in the case of a less hydrophobic surface. The transitional state [42] of the droplet between CB and Wenzel wetting defines hydrophobicity of the printed surface.

Apart from wetting properties, surface coloration is another result of the surface structure. Iridescence - the hue of surface is varied by changing the viewing angle - is sought after in marking, security against counterfeiting and jewelry. In butterflies, iridescence is responsible for producing attractive colors [11,12,23]. In flowers, it provides a cue to animal pollinators [43]. Structures that produce iridescent colors are classified into three types: multilayer reflectors, three dimensional photonic crystals, and diffraction gratings. The structure shown in Fig. 2(a) has parallel ridges resembling a diffraction grating with a color appearance due to diffraction. The iridescence from the diffraction gratings is different from the other types of structures as the colors are ordered from red to violet for observer at a fixed observation angle according to the grating equation:

$$d(\sin\theta_r - \sin\theta_i) = m\lambda, \quad (3)$$

where d is the period of the gratings, θ_i is the angle of incidence, θ_r is the angle of reflection of the diffraction order m, and λ is the wavelength of light. The flashy and shimmering colors: blue, green, orange and red are clearly observed as the viewing angle is gradually change (bottom of Fig. 4(a)).

In addition to the striking iridescence of such printed textured surfaces, polarization and directionality of reflection are expected to be pronounced as exhibited by several biological species. The structural color reflection from the shell of mollusk Helcion pruinosus [44] and on the wing of moth Trichoplusia orichalcea [25] is found to be highly directional. The structure of the wing (inset Fig. 4(a)) is composed of raised ridges connected together by a herringbone pattern of microribs. This arrangement of the wing structure was reproduced by the proposed printing (Fig. 4(a)).

On the basis of diffraction theory Straton-Silver-Chu integral [45,46], a theoretical model of the complex diffracting wing structure of *Trichoplusia orichalcea* to predict its polarization, directionality of reflection and color properties was developed [25]. It was found by calculation and experiment that under the condition of specular reflection (the angle of incidence equal to the angle of diffraction), the diffraction intensity has a strong dependence on the angle of incidence and on the azimuthal orientation of the wing. Same analysis of the diffraction intensity and the wing orientation for the printed structures is shown in Fig. 4(b). The sample was mounted on a turning table which could be rotated around the y-axis to select different values of incidence angles Θ_i and also the azimuthal orientation was chosen by rotating around z-axis Θ_r (Supplementary Figure S5). The sample was initially aligned along the line OA (parallel to the micro scale ridges: $\Theta_r = 0°$). The linear polarizers were placed in the path of both incident and reflected beams to record the same S-type or P-type diffracted powers at 633 nm wavelength. The diffracted power for the incidence angles of 45° and 60° under the condition of specular reflection for both S and P

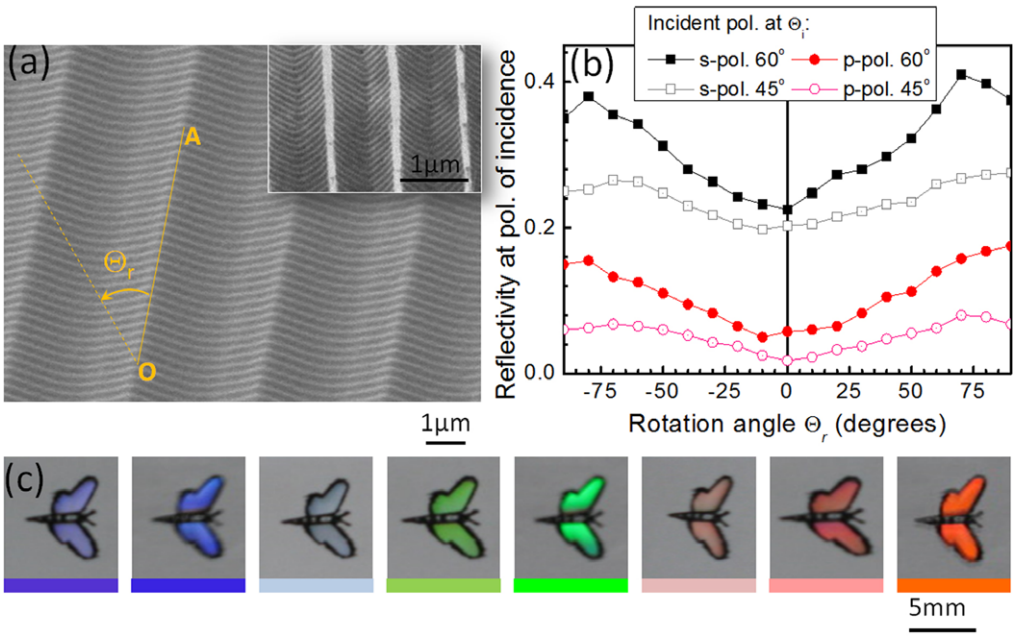

Figure 4 Optical properties of hierarchical surfaces. (a) SEM micrograph of the fabricated hierarchical structure mimicking the wing of the moth Trichoplusia orichalcea [19] (inset in (a) shows SEM image of the actual moth wing; scale bar 1 μm). The larger gratings have a period of 3 μm while the smaller is 300 nm. (b) Dependence of the diffracted power on the orientation of the mimicked wing structure (rotation in the plane of the sample). The rotation angle $\Theta_r = 0°$ for the line OA (shown in (a)) corresponds to the vertical orientation. The measured results for both S and P polarized light for the incidence angles of 45° and 60° at the wavelength of 630 nm. The units on the y-axis are normalized to the direct power measured without reflection from the sample. (c) Colors of the visible spectrum from violet to red caused by iridescence by gradually lowering the viewing angle.

polarizations (Fig. 4(b)) showed that the diffraction intensity was increasing along the angle of incidence from 45° to 60° for both polarizations.

The presented results agree to a high degree with the theoretical predictions and experimental findings for the real wing structure of the moth *Trichoplusia orichalce* [25]. When the orientation of the structure was changed from $+90°$ to $-90°$ in the azimuthal orientation, it corresponds to the path swapping betwen the incident and diffracted beams. For the all incidence angles it was found that S polarized light diffracted significantly stronger as compared with P polarization. So, under non-polarised illumination of natural light the structure can act as a linear polarizer with a high efficiency depending on the orientation angle Θ_r.

4. Conclusions and outlook

We have demonstrated the multiple exposure of two beam laser interference with angle variation and period modulation as a potential technique for direct printing of biomimetic hierarchical structures. Based on sequence of exposures, orientation angle of the sample and period of interference pattern, a variety of multiscale surfaces with geometrically symmetrical structures has been be produced. It has been shown experimentally that the obtained structures can be used to mimic several natural phenomena: super hydrophobicity, iridescence, directionality of reflectivity, and polarization at different colors. The approach used here can be applied to fabricate biomimetic surfaces which can find potential applications in wide range of disciplines of microfluidics, antifouling, decorative/holographic elements, colored jewelry, micro/nano optics, polarizing filters and surface enhanced Raman scattering sensors. The proposed method of surface printing can be easily adopted for randomized patterns which produce new functionalities, such as the low reflectivity and wide angular selectivity. Surfaces for thermal management of light at IR wavelength using Wolf's effect can be made for narrow band emitters [47].

Supporting Information

Additional supporting information may be found in the online version of this article at the publisher's website.

Acknowledgements. This work was supported by the National Natural Science Foundation of China and National 973 Program under Grants # 61590930, 61435005, 2014CB921302, 51335008, and 61378053.

Received: 11 July 2016, **Revised:** 18 December 2016, **Accepted:** 19 December 2016

Published online: 13 January 2017

Key words: Hierarchical structures, 3D printing, biomimetics, laser fabrication.

References

[1] W. Barthlott and C. Neinhuis, Planta **202**, 1–8 (1997).
[2] P. Ball, Nature **400**, 507–509 (1999).
[3] L. Wen, J. C. Weaver, P. J. Thornycroft, and G. V. Lauder, Bioinspir. Biomim. **10**, 066010 (2015).
[4] D. Wu, J. N. Wang, S. Z. Wu, Q. D. Chen, S. Zhao, H. Zhang, H. B. Sun, and L. Jiang, Adv. Funct. Mater. **21**, 2927–2932 (2011).
[5] L. Feng, Y. Zhang, J. Xi, Y. Zhu, N. Wang, F. Xia, and L. Jiang, Langmuir **24**, 4114–4119 (2008).
[6] B. B. Xu, Y. L. Zhang, W. Y. Zhang, X. Q. Liu, J. N. Wang, X. L. Zhang, D. D. Zhang, H. B. Jiang, R. Zhang, and H. B. Sun, Adv. Opt. Mater. **1**, 56–60 (2013).
[7] X. Gao and L. Jiang, Nature **432**, 36 (2004).
[8] Q. Wang, X. Yao, H. Liu, D. Quéré, and L. Jiang, PNAS **112**, 9247–9252 (2015).
[9] X. Gao, X. Yan, X. Yao, L. Xu, K. Zhang, J. Zhang, B. Yang, and L. Jiang, Adv. Mater. **19**, 2213–2217 (2007).
[10] K. Autumn, Y. A. Liang, S. T. Hsieh, W. Zesch, W. P. Chan, T. W. Kenny, R. Fearing, and R. J. Full, Nature **405**, 681–685 (2000).
[11] H. Ghiradella, Appl. Opt. **30**, 3492–3500 (1991).
[12] D. G. Stavenga, H. L. Leertouwer, D. C. Osorio, and B. D. Wilts, Light Sci. Appl. **4**, e243 (2015).
[13] B. Bhushan, K. Koch, and C. J. Yong, Ultramicroscopy **109**, 1029–1034 (2009).
[14] X. Yao, Q. Chen, L. Xu, Q. Li, Y. Song, X. Gao, D. Quéré, and L. Jiang, Adv. Funct. Mater. **20**, 656–662 (2010).
[15] L. Feng, Y. Zhang, M. Li, Y. Zheng, W. Shen, and L. Jiang, Langmuir **26**, 14885–14888 (2010).
[16] A. K. Geim, S. V. Dubonos, I. V. Grigorieva, K. S. Novoselov, A. A. Zhukov, and S. Y. Shapoval, Nat. Mater. **2**, 461–463 (2003).
[17] K. Watanabe, T. Hoshino, K. Kanda, Y. Haruyama, and S. Matsui, Jpn. J. Appl. Phys. **44**, L48-L50 (2004).
[18] D. Wu, Q. D. Chen, H. Xia, J. Jiao, B. B. Xu, X. F. Lin, Y. Xu, and H. B. Sun, Soft Matter **6**, 263–267 (2010).
[19] S. J. Choi, M. K. Choi, D. Tahk, and H. Yoon, J. Mater. Chem. **21**, 14936–14940 (2011).
[20] F. Zhang, J. Chan, and H. Y. Low, Appl. Surf. Sci. **254**, 2975–2979 (2008).
[21] C. Neinhuis and W. Barthlott, Ann. Bot. **79**, 667–677 (1997).
[22] M. Liu, S. Wang, and L. Jiang, Mrs Bull. **38**, 375–382 (2013).
[23] P. Vukusic, J. R. Sambles, and C. R. Lawrence, Nature **404**, 457 (2000).
[24] R. Brunner, O. Sandfuchs, C. Pacholski, C. Morhard, and J. Spatz, Laser Photonics Rev. **6**, 641–659 (2012).
[25] D. J. Brink, J. E. Smit, M. E. Lee, and A. Möller, Appl. Opt. **34**, 6049–6057 (1995).
[26] J. K. Oh, X. Lu, Y. Min, L. Cisneros-Zevallos, and M. Akbulut, Acs Appl. Mater. Inter. **7**, 19274–19281 (2015).
[27] Z. Sun, T. Liao, K. Liu, L. Jiang, J. H. Kim, and S. X. Dou, Small **10**, 3001–3006 (2014).
[28] D.-J. Guo, R. Liu, Y. Cheng, H. Zhang, L.-M. Zhou, S.-M. Fang, W. H. Elliott, and W. Tan, Acs Appl. Mater. Inter. **7**, 5480–5487 (2015).
[29] Y. L. Kong, M. K. Gupta, B. N. Johnson, and M. C. McAlpine, Nano Today **11**, 330–350 (2016).
[30] Y. Jie, Q. Jiang, Y. Zhang, N. Wang, and X. Cao, Nano Energy **27**, 554–560 (2016).
[31] J. Yang, F. Luo, T. S. Kao, X. Li, G. W. Ho, J. Teng, X. Luo, and M. Hong, Light Sci. Appl. **3**, e185 (2014).
[32] K. Golovin, D. H. Lee, J. M. Mabry, and A. Tuteja, Angew Chem. Int. Edit. **52**, 13007–13011 (2013).
[33] J. N. Wang, Y. L. Zhang, Y. Liu, W. Zheng, L. P. Lee, and H. B. Sun, Nanoscale **7**, 7101–7114 (2015).
[34] T. P. N. Nguyen, R. Boukherroub, V. Thomy, and Y. Coffinier, J. Colloid Interf. Sci. **416**, 280–288 (2014).
[35] M. Malinauskas, A. Zukauskas, S. Hasegawa, Y. Hayasaki, V. Mizeikis, R. Buividas, and S. Juodkazis, Light Sci Appl. **5**, e16133 (2016).
[36] G. M. Burrow and T. K. Gaylord, Micromachines **2**, 221–257 (2011).
[37] N. D. Lai, W. P. Liang, J. H. Lin, C. C. Hsu, and C. H. Lin, Opt. Express **13**, 9605–9611 (2005).
[38] L. Wang, Z.-H. Lu, X.-F. Lin, Q.-D. Chen, B.-B. Xu, and H.-B. Sun, J. Lightwave Technol. **31**, 276–281 (2013).
[39] Y. T. Cheng, D. E. Rodak, C. A. Wong, and C. A. Hayden, Nanotechnology **17**, 1359–1362 (2006).
[40] R. N. Wenzel, Ind. Eng. Chem. **28**, 988–994 (1936).
[41] A. B. D. Cassie, Discuss Faraday Soc. **3**, 11–16 (1948).
[42] S. Wang and L. Jiang, Adv. Mater. **19**, 3423–3424 (2007).
[43] H. M. Whitney, M. Kolle, P. Andrew, L. Chittka, U. Steiner, and B. J. Glover, Science **323**, 130–133 (2009).
[44] D. J. Brink, V. D. B. Ng, and A. J. Botha, Appl. Opt. **41**, 717–722 (2002).
[45] S. Silver, Microwave antenna theory and design, (McGraw-Hill, New York, 1947).
[46] R. M. A. Azzam and N. M. Bashara, Phys. Rev. B. **5**, 4721–4729 (1972).
[47] J. J. Greffet, R. Carminati, K. Joulain, J. P. Mulet, S. Mainguy, and Y. Chen, Nature **416**, 61–64 (2002).